# Practical Design Approach to Microstrip Combline-Type Filters

ARPAD D. VINCZE, MEMBER, IEEE

***Abstract*—A general circuit model resembling a combline-type structure is developed using the concept of self and mutual node admittances rather than self and mutual capacitances per unit length. The merit of this approach lies in the relative simplicity of design formulas readily applicable to filters utilizing microstrip or stripline construction. It also offers easy adaptability to computer aided design. Equations are derived relating even–odd mode impedances and transmission line lengths to prototype elements and other design parameters.**

## NOMENCLATURE

| | |
|---|---|
| $n$ | Order of low pass prototype filter. |
| $g_0,g_1\cdots g_{n+1}$ | Elements of the low pass prototype filter. |
| $w$ | Fractional bandwidth $= (f_2 - f_1)/f_0$, where $f_2$ and $f_1$ are 3 dB or equiripple points and $f_0$ is the center frequency. |
| $J_{j,j+1}$ | Admittance inverter between nodes $j$ and $j+1$. |
| $b_j$ | Resonant slope parameter at node $j$. |
| $B_j$ | Total resonant susceptance at node $j$. |
| $B_{0,1}{}^{c,s}$ | Coupled and self susceptances from nodes 0 and 1, respectively. |
| $B_{n+1}{}^{c}$ | Coupled susceptance from node $n+1$. |
| $C_{A1},C_{B1},C_{An},C_{Bn}$ | Tapped capacitances of type I filters. |
| $\bar{Z}$ | Average mode impedance of resonator stubs. |
| $Z_j$ | Tuning stub line characteristic impedance (types IIa and Ia). |
| $C_j$ | Resonator tuning capacitance (types Ib and IIb). |
| $\phi$ | Resonator stub line length. |
| $\theta$ | Tuning stub line length. |
| $R_A,R_B$ | Terminating impedances at nodes 0 and $n+1$. |
| $R = 1/G$ | Uptransformed impedance across resonant nodes 1 and $n$. |
| $a_{j,j+1}$ | Coupling factor between nodes $j$ and $j+1$. |
| $\gamma_1,\gamma_n$ | Constants associated with coupled susceptances at nodes 1 and $n$ of type II filter ($\geq 1$). |
| $c_1,k_1,c_n,k_n$ | Constants associated with coupled susceptance at nodes 1 and $n$ of type I filter ($\leq 1$). |
| $X_S/R_A$ | Impedance ratio for type I filter, less than one, usually chosen 0.5 or less. |
| $T$ | Ideal transformer impedance transformation ratio ($\leq 1$) for type I filters. |
| $N$ | Ideal transformer impedance transformation ratio ($\geq 1$) for type II filters. |

Manuscript received May 16, 1974; revised August 28, 1974.
The author is with Philco Western Development Laboratories, Philco-Ford Company, Palo Alto, Calif. 94303.

## I. INTRODUCTION

THE advancement of microminiaturization and thick–thin-film technology resulted in increased utilization of microstrip construction. A good wealth of design information is available for high dielectric substrate characterization [5], [6] along with the fundamentals of filter theory laid down earlier [1]–[3], [7], [8], [10]. All this is applied to develop new and practical filter designs on microstrip.

One example is the parallel-coupled half-wave filter developed earlier [2]. The filter discussed here is quite different from that in appearance and performance; it may be considered, however, as one followup to the half-wave parallel-coupled filter because of similarities in design approach and application. There are, of course, differences and limitations as well.

One basic limitation is that the low pass prototype elements should be symmetrical or antimetric. This, however, is not considered a serious shortcoming since most designs call for this condition. The source and load impedances ($R_A,R_B$) are not required to be equal, although they are in most practical cases. All intermediate coupled resonator stubs ($j = 2$ to $n-1$) have the same width; the spacing between coupled stub pairs is a variable parameter directly related to the coupling factor "$a$." Fig. 1 shows the four basic filter types to be discussed. Type I uses capacitive-tapped while type II parallel-coupled end sections. Two special cases are considered: 1) when only the series capacitors $C_{A1}$ and $C_{An}$ are used; and 2) when the end coupler line pairs have equal strip widths. Both cases introduce one degree of simplicity into the design.

The resonator stubs are tuned by high impedance tuning lines that are assumed to have zero mutual coupling. They introduce an attenuation pole frequency in the upper stopband in addition to the one introduced by the coupled resonator stubs. This improves the ultimate attenuation to some extent and results in steeper skirt on the upper side. The stray coupling between tuning lines causes wider bandwidth than designed for; five solutions are suggested to minimize this discrepancy.

The principles and conditions upon which the design

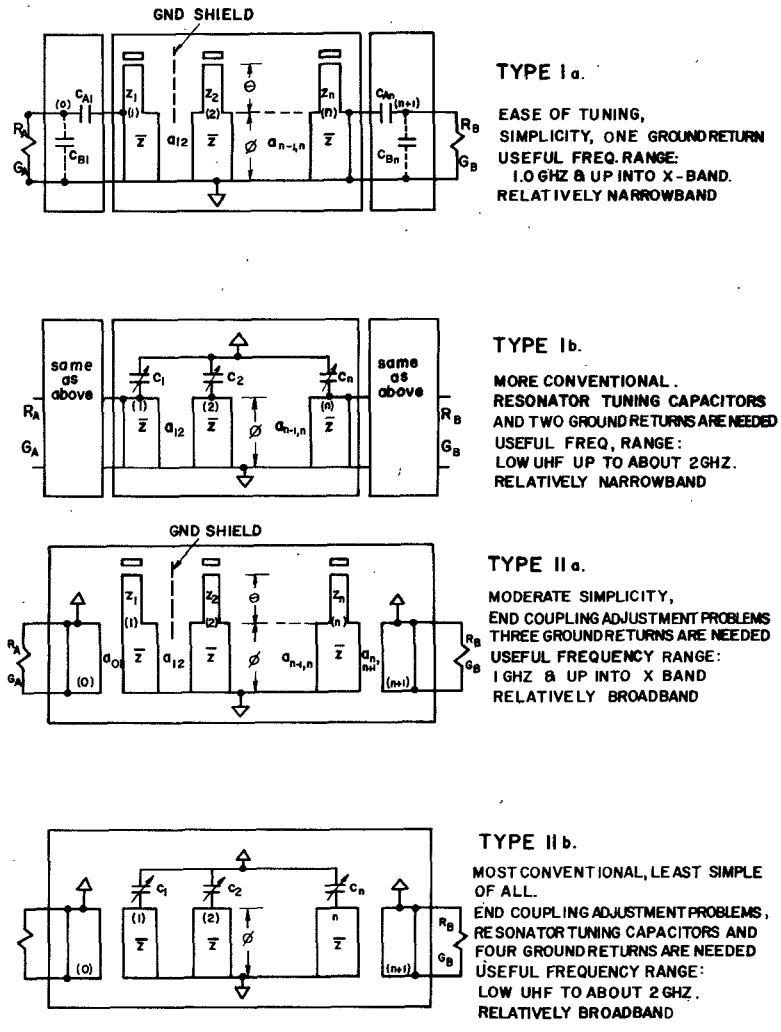


Fig. 1. Four basic types of combline filter configurations realizable with microstrip or stripline construction.

equations are based are discussed; the advantages and disadvantages of the two types are examined emphasizing the objectives in choosing the proper one to fit requirements. One special case associated with each filter type is discussed. Resonance conditions and slope parameters are derived for the external and internal nodes.

Practical examples are presented to compare theoretical and test data for a three-pole filter. Computed response is plotted and a computer flow chart is shown to illustrate the sequence of the iterative design computation process.

All fundamental concepts and equations pertinent to this design are treated in the Appendix; it is shown there how the intermediate resonant nodes and inverters are formed to give the semilumped element ladder structures of Fig. 2.

## II. DEVELOPMENT OF DESIGN RELATIONSHIPS

The foundation of development for the design equations is based largely on the theory of direct coupled resonator filters developed earlier by Cohn [3]. The basic formulas in Table I are applicable directly to the admittance-inverter configuration presented herein and they are utilized to derive the design equations in Tables II and III.

Consider the schematic representation of the four filter types shown on Fig. 1 along with the component designations. The resonator stubs are characterized by $\bar{Z}$ [defined by (A3)] and tuned to resonance by high impedance open line stubs of characteristic impedances $Z_1 \cdots Z_n$ at each node. While coupling is specified between the parallel resonator stubs, it is assumed zero between the tuning lines. This assumption is indicated by the "ground shield" between line pairs as shown on the figure. In practice, there is some coupling there whose effect may be minimized by: 1) designing for narrower bandwidth initially; 2) choosing the tuning line impedances 2–3 times as high as $\bar{Z}$; 3) bending the tuning lines away from each other; 4) eliminating $Z_1$ and $Z_n$ in the type I structure by resonating the end stubs solely with $C_{A1}$, $C_{B1}$ and $C_{An}$, $C_{Bn}$; and 5) providing a ground shield between tuning lines to terminate stray coupling. This may be effective but the costliest of all. As the number of poles exceeds four, it becomes more difficult to minimize stray coupling without a ground shield.

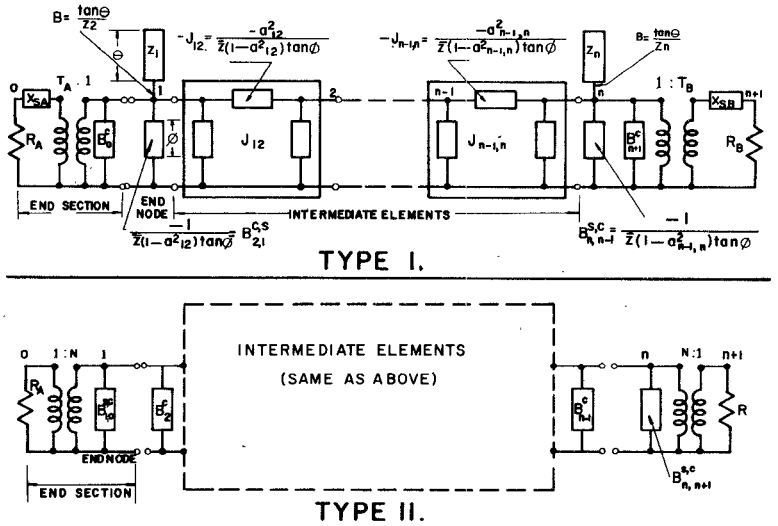


Fig. 2. Equivalent circuits for types I and II filters.

TABLE I
INVERTER–RESONATOR RELATIONSHIPS FOR THE PARALLEL RESONANT MODE (FROM [3])

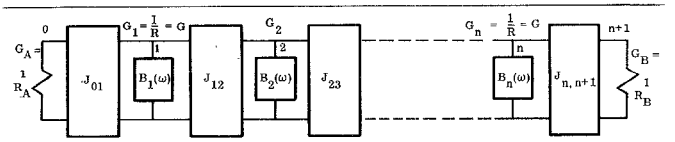

$G_1, G_2 \ldots G_n$ = impedance levels at the resonant nodes.

$$b_j = \frac{\omega_0}{2} \frac{d\,B_j(\omega)}{d\omega}\bigg|_{\omega=\omega_0} \text{ mho} \tag{1}$$

$$J_{01} = \sqrt{\frac{G_A b_1 w}{g_0 g_1}} \tag{2}$$

$$J_{n,n+1} = \sqrt{\frac{G_B b_n w}{g_n g_{n+1}}} \tag{3}$$

$$J_{j,j+1} = \sqrt{\frac{G_B b_n w}{g_n g_{n+1}}} \quad j = 1 \text{ to } n-1 \tag{4}$$

$$\frac{b_1}{G} = \frac{g_0 g_1}{w} \tag{5}$$

$$\frac{b_n}{G} = \frac{g_n g_{n+1}}{w} \tag{6}$$

$$G = \frac{J_{01}^2}{G_A} = \frac{J_{n,n+1}^2}{G_B} \tag{7}$$

The coupling between resonator stubs $j$ and $j+1$ is expressed by $a_{j,j+1}$, the coupling factor defined by (A4). To obtain the desired response, the spacing between resonators is adjusted while the resonator widths are held the same. This results in simpler equations and easier less costly product design.

The basic difference between types I and II is the end section used. There are certain advantages and disadvantages associated with each type. For example, the parallel-coupled end section of type II can transform a constant impedance over a broad bandwidth using the special constraint $Y_{00}^a + Y_{0e}^a = 2G_A$. The price paid for using this type is increased complexity and gap tolerance problems due to high coupling factors. (It is often difficult to realize coupling factors greater than 0.25 and in many cases, readjustment of the end couplers is necessary to improve performance.) However, discreet components are not used to advantage, but line elements only; thus extension of the design up to $X$ band is quite possible.

The special case of the parallel-coupled end section is when both lines have equal widths. This occurs for one particular end node impedance level $R°$. To change $R°$

## TABLE II

### COMBLINE FILTER DESIGN WITH PARALLEL-COUPLED END SECTIONS

| | TYPE IIa | | TYPE IIb | |
|---|---|---|---|---|
| | 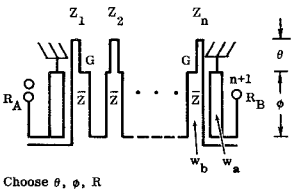 Choose $\theta$, $\phi$, R | | 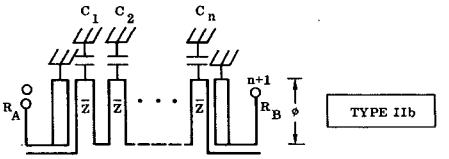 Choose $\phi$, R | |
| | | Special Case: equal width coupling at ends | | Special Case: equal width coupling at ends |
| (1) $F(\theta,\varphi)$ | $\frac{2\phi}{\sin 2\phi} + \frac{2\theta}{\sin 2\theta}$ | | $F(\phi) = \frac{2\phi}{\sin 2\phi} + 1$ | |
| (2) $R^o$ | | $R^o \cong R_A\left[1 + \frac{2g_0g_1 \tan\phi}{w\ F(\theta,\phi)}\right]$ | | $R^o \cong R_A\left[1 + \frac{2g_0g_1 \tan\phi}{w\ F(\phi)}\right]$ |
| (3) $\bar{Z}$ $(g_0g_1 = g_ng_{n+1})$ | $\frac{wR\,F(\theta,\phi)}{2g_0g_1\,\bar{\gamma}\left[1 - \left(\bar{a}^2 + a_{12}^2\right)\right]\tan\phi}$ | $\bar{Z}^o = \frac{R^oR_A}{R^o - R_A}$ | $\frac{wR\,F(\phi)}{2g_0g_1\,\bar{\gamma}\left[1 - \left(\bar{a}^2 + a_{12}^2\right)\right]\tan\phi}$ | $Z^o = \frac{R^oR_A}{R^o - R_A}$ |
| (4) $a_{01}$ | $1\Big/\sqrt{2 + \frac{RR_A}{\bar{Z}^2}}$ | $\sqrt{\frac{R_A}{R^o}}$ | $1\Big/\sqrt{2 + \frac{RR_A}{\bar{Z}^2}}$ | $\sqrt{\frac{R_A}{R^o}}$ |
| (5) $a_{n+1,n}$ | $1\Big/\sqrt{2 + \frac{RR_B}{\bar{Z}^2}}$ | $\sqrt{\frac{R_B}{R^o}}$ | $1\Big/\sqrt{2 + \frac{RR_B}{Z^2}}$ | $\sqrt{\frac{R_B}{R^o}}$ |
| (6) $\gamma_1$ | $\frac{1}{1 - \frac{R_A}{\bar{Z}} \cdot \frac{a_{01}^2}{1 - a_{01}^2}}$ | $\frac{1}{1 - \frac{R_A}{\bar{Z}^o} \cdot \frac{a_{01}^2}{1 - a_{01}^2}}$ | $\frac{1}{1 - \frac{R_A}{\bar{Z}} \cdot \frac{a_{01}^2}{1 - a_{01}^2}}$ | $\frac{1}{1 - \frac{R_A}{\bar{Z}^o} \cdot \frac{a_{01}^2}{1 - a_{01}^2}}$ |
| (7) $\gamma_n$ | $\frac{1}{1 - \frac{R_B}{\bar{Z}} \cdot \frac{a_{n+1,n}^2}{1 - a_{n+1,n}^2}}$ | $\frac{1}{1 - \frac{R_B}{\bar{Z}^o} \cdot \frac{a_{n+1,n}^2}{1 - a_{n+1,n}^2}}$ | $\frac{1}{1 - \frac{R_B}{\bar{Z}} \cdot \frac{a_{n+1,n}^2}{1 - a_{n+1,n}^2}}$ | $\frac{1}{1 - \frac{R_B}{\bar{Z}^o} \cdot \frac{a_{n+1,n}^2}{1 - a_{n+1,n}^2}}$ |
| (8) $\bar{\gamma}$ | $\frac{\gamma_1 + \gamma_n}{2}$ | | | |
| (9) $\bar{a}$ | $\frac{a_{01} + a_{n+1,n}}{2}$ | | | |
| (10) $Z_1$ | $\gamma_1\bar{Z}\left[1 - \left(a_{01}^2 + a_{12}^2\right)\right]\tan\theta\tan\phi$ | $\gamma_1\bar{Z}^o\left[1 - \left(a_{01}^2 + a_{12}^2\right)\right]\tan\theta\tan\phi$ | $\frac{1}{\omega_0C_1} = \gamma_1\bar{Z}\left[1 - \left(a_{01}^2 + a_{12}^2\right)\right]\tan\phi$ | $\frac{1}{\omega_0C_1} = \gamma_1\bar{Z}^o\left[1 - \left(a_{01}^2 + a_{12}^2\right)\right]\tan\phi$ |
| (11) $Z_n$ | $\gamma_n\bar{Z}\left[1 - \left(a_{n+1,n}^2 + a_{n-1,n}^2\right)\right]\tan\theta\tan\phi$ | $\gamma_n\bar{Z}^o\left[1 - \left(a_{n+1,n}^2 + a_{n-1,n}^2\right)\right]\tan\theta\tan\phi$ | $\frac{1}{\omega_0C_n} = \gamma_n\bar{Z}\left[1 - \left(a_{n+1,n}^2 + a_{n-1,n}^2\right)\right]\tan\phi$ | $\frac{1}{\omega_0C_1} = \gamma_n\bar{Z}^o\left[1 - \left(a_{n+1,n}^2 + a_{n-1,n}^2\right)\right]\tan\phi$ |
| (12) $a_{12} = a_{n-1,n}$ $(g_1g_2 = g_ng_{n+1})$ | $\frac{wF(\theta,\phi)}{2\sqrt{\bar{\gamma}g_1g_2}}\left[1 + \frac{\bar{a}^2 + a_{23}^2}{2}\right]$ | | $\frac{wF(\phi)}{2\sqrt{\bar{\gamma}g_1g_2}}\left[1 + \frac{\bar{a}^2 + a_{23}^2}{2}\right]$ | |
| (13) $a_{10}$ | $\sqrt{\frac{R_A}{R}}$ | | | |
| (14) $a_{n,n+1}$ | $\sqrt{\frac{R_B}{R}}$ | | | |
| (15) $a_{j,j+1}$ | $\frac{wF(\theta,\phi)}{2\sqrt{g_jg_{j+1}}}\left[1 + \frac{a_{j-1,j}^2 + a_{j+2,j+1}^2}{2}\right]$, j = 2 to n-2 | | $\frac{wF(\phi)}{2\sqrt{g_jg_{j+1}}}\left[1 + \frac{a_{j-1,j}^2 + a_{j+2,j+1}^2}{2}\right]$, j = 2 to n-2 | |
| (16) $Z_j, C_j$ | $\bar{Z}\tan\theta\tan\phi\left[1 - \left(a_{j-1,j}^2 + a_{j,j+1}^2\right)\right]$, j = 2 to n-1 | | $\frac{1}{\omega_0C_j} = \bar{Z}\tan\phi\left[1 - \left(a_{j-1,j}^2 + a_{j,j+1}^2\right)\right]$, j = 2 to n-1 | |
| (17) $Z_{oe\,j,j+1}$ $Z_{oo\,j,j+1}$ | $Z_{oe\,j,j+1} = \bar{Z}(1 + a_{j,j+1})$, $Z_{oo\,j,j+1} = \bar{Z}(1 - a_{j,j+1})$, j = 0 to n | | | |

## TABLE III
### Combline Filter Design with Capacitive-Tapped End Sections

| | TYPE Ia | | TYPE Ib | |
|---|---|---|---|---|
| | 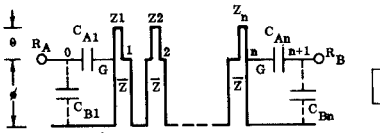 Choose: $X_{s1}/R_A$, $\theta$, $\phi$, G, (Let $X_{s1}/R_A = X_{sn}/R_B$) $G = 1/R$ | Special Case: $C_{B1} = C_{Bn} = 0$ | 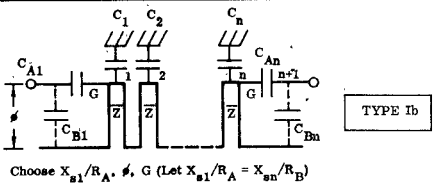 Choose $X_{s1}/R_A$, $\phi$, G (Let $X_{s1}/R_A = X_{sn}/R_B$) | Special Case: $C_{B1} = C_{Bn} = 0$ |
| (1) $F(\theta,\phi)$ | $\frac{2\phi}{\sin 2\phi} + \frac{2\theta}{\sin 2\theta}$ | | $F(\phi) = \frac{2\phi}{\sin 2\phi} + 1$ | |
| (2) $T_1$ | $\sqrt{(R_A/R)\left[1 + (X_{s1}/R_A)^2\right]}$ | 1 | $\sqrt{(R_A/R)\left[1 + (X_{s1}/R_A)^2\right]}$ | 1 |
| (3) $T_n$ | $\sqrt{(R_B/R)\left[1 + (X_{sn}/R_B)^2\right]}$ | 1 | $\sqrt{(R_B/R)\left[1 + (X_{sn}/R_B)^2\right]}$ | 1 |
| (4) $B_o^c$ | $-\frac{X_{s1}}{R_A}\left[\frac{1}{R} + \frac{R_A T_1 (1 - T_1)}{X_{s1}^2}\right]$ | $+ G\sqrt{\frac{G_A}{G} - 1}$ | $-\frac{X_{s1}}{R_A}\left[\frac{1}{R} + \frac{R_A T_1 (1 - T_1)}{X_{s1}^2}\right]$ | $+ G\sqrt{\frac{G_A}{G} - 1}$ |
| (5) $B_{n+1}^c$ | $-\frac{X_{sn}}{R_B}\left[\frac{1}{R} + \frac{R_B T_B (1 - T_B)}{X_{sn}^2}\right]$ | $+ G\sqrt{\frac{G_B}{G} - 1}$ | $-\frac{X_{sn}}{R_B}\left[\frac{1}{R} + \frac{R_B T_n (1 - T_n)}{X_{sn}^2}\right]$ | $+ G\sqrt{\frac{G_B}{G} - 1}$ |
| (6) $k_1$, $k_n$ | $k_1 = \frac{(B_o^c)\frac{wR}{2g_0g_1} F(\theta,\phi)}{\cot\theta\left[1 - (B_o^c)\frac{wR}{2g_0g_1}\cdot\frac{2\phi}{\sin 2\phi}\right]}$, $k_n = \frac{(B_{n+1}^c)\frac{wR}{2g_ng_{n+1}} F(\theta,\phi)}{\cot\theta\left[1 - (B_{n+1}^c)\frac{wR}{2g_ng_{n+1}}\cdot\frac{2\phi}{\sin 2\phi}\right]}$ | | $k_1 = \frac{(B_o^c)\frac{wR}{2g_0g_1} F(\phi)}{1 - (B_o^c)\frac{wR}{2g_0g_1}\cdot\frac{2\phi}{\sin 2\phi}}$, $k_n = \frac{(B_{n+1}^c)\frac{wR}{2g_ng_{n+1}} F(\phi)}{1 - (B_{n+1}^c)\frac{wR}{2g_ng_{n+1}}\cdot\frac{2\phi}{\sin 2\phi}}$ | |
| (7) $Z_1$, $Z_n$ or $C_1$, $C_n$ | $Z_1 = k_1/B_o^c$, $Z_n = k_n/B_{n+1}^c$ | | $C_1 = \frac{B_o^c}{k_1\omega_0}$, $C_n = \frac{B_{n+1}^c}{k_n\omega_0}$ | |
| (8) $c_1$, $c_n$ | $c_1 = \frac{1}{1 + k_1\cot\theta}$, $c_n = \frac{1}{1 + k_n\cot\theta}$ | | $c_1 = \frac{1}{1 + k_1}$, $c_n = \frac{1}{1 + k_n}$ | |
| (9) $\bar{c}$ | $\frac{c_1 + c_n}{2}$ | | | |
| (10) $F(\theta,\phi,\bar{c})$ | $\frac{2\phi}{\sin 2\phi} + \frac{2\theta}{\sin 2\theta}\cdot\bar{c}$ | | $F(\phi,\bar{c}) = \frac{2\phi}{\sin 2\phi} + \bar{c}$ | |
| (11) $\bar{Z}$ | $\frac{wR\,F(\theta,\phi,\bar{c})}{2g_0g_1\left(1 - a_{12}^2\right)\tan\phi}$, $(g_0g_1 = g_ng_{n+1})$ | | $\frac{wR\,F(\phi,\bar{c})}{2g_0g_1\left(1 - a_{12}^2\right)\tan\phi}$, $(g_0g_1 = g_ng_{n+1})$ | |
| (12) $a_{12} = a_{n-1,n}$ | $\frac{w\sqrt{F(\theta,\phi,\bar{c})\,F(\theta,\phi)}}{2\sqrt{g_1g_2}}$, $(g_1g_2 = g_{n-1}g_n)$ | | $\frac{w\sqrt{F(\phi,\bar{c})\,F(\phi)}}{\sqrt{2\ g_1g_2}}$, $(g_1g_2 = g_{n-1}g_n)$ | |
| (13) $a_{j,j+1}$ | $\frac{wF(\theta,\phi)}{2\sqrt{g_jg_{j+1}}}\left[1 + \frac{a_{j-1,j}^2 + a_{j+2,j+1}^2}{2}\right]$, j = 2 to n-2 | | $\frac{F(\theta,\phi)}{2\sqrt{g_jg_{j+1}}}\left[1 + \frac{a_{j-1,j}^2 + a_{j+2,j+1}^2}{2}\right]$, j = 2 to n-2 | |
| (14) $Z_j$ | $\bar{Z}\tan\theta\tan\phi\left[1 - \left(a_{j-1,j}^2 + a_{j,j+1}^2\right)\right]$, j = 2 to n-2 | | | |
| (15) $Z_{oe\,j,j+1}$, $Z_{oo\,j,j+1}$ | $Z_{oe\,j,j+1} = \bar{Z}(1 + a_{j,j+1})$, $Z_{oo\,j,j+1} = \bar{Z}(1 - a_{j,j+1})$, j = 0 to n | | | |
| (16) $C_{A1}$, $C_{An}$ | $C_{A1} = \frac{T_1}{\omega_0X_{s1}}$, $C_{An} = \frac{T_n}{\omega_0X_{sn}}$ | $C_{A1} = \frac{GG_A}{B_o^c\omega_0}$, $C_{An} = \frac{GG_B}{B_{n+1}^c\omega_0}$ | $C_{A1} = \frac{T_1}{\omega_0X_{s1}}$, $C_{An} = \frac{T_n}{\omega_0X_{sn}}$ | $C_{A1} = \frac{GG_A}{B_o^c}$, $C_{An} = \frac{GG_B}{B_{n+1}^c}$ |
| $C_{B1}$, $C_{Bn}$ | $C_{B1} = \frac{1 - T_1}{\omega_0X_{s1}}$, $C_{Bn} = \frac{1 - T_n}{\omega_0X_{sn}}$ | | $C_{B1} = \frac{1 - T_1}{\omega_0X_{s1}}$, $C_{Bn} = \frac{1 - T_n}{\omega_0X_{sn}}$ | |

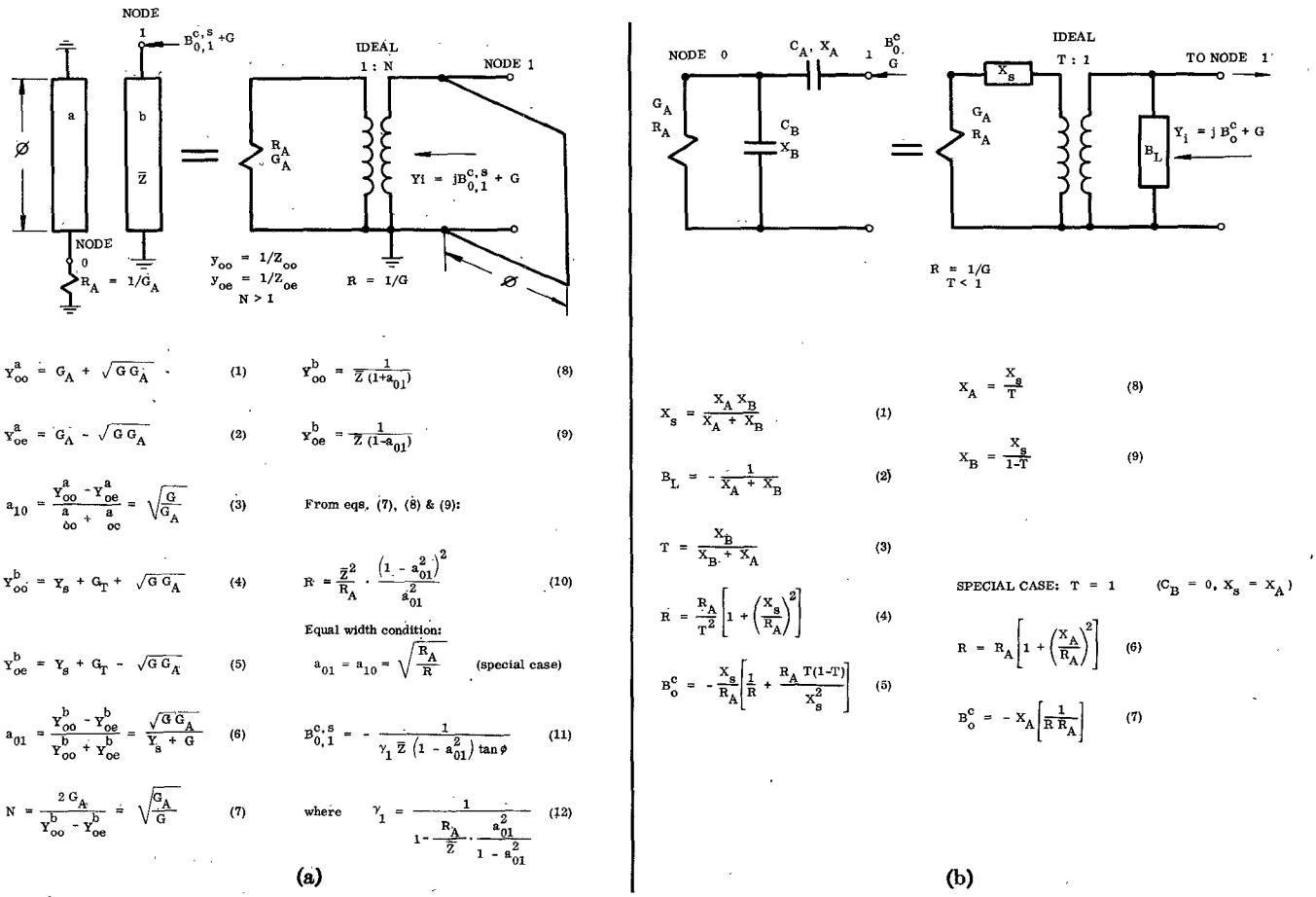


$$Y_{oo}^a = G_A + \sqrt{G G_A} \quad (1)$$

$$Y_{oe}^a = G_A - \sqrt{G G_A} \quad (2)$$

$$a_{10} = \frac{Y_{oo}^a - Y_{oe}^a}{Y_{oo}^a + Y_{oe}^a} = \sqrt{\frac{G}{G_A}} \quad (3)$$

$$Y_{oo}^b = Y_s + G_T + \sqrt{G G_A} \quad (4)$$

$$Y_{oe}^b = Y_s + G_T - \sqrt{G G_A} \quad (5)$$

$$a_{01} = \frac{Y_{oo}^b - Y_{oe}^b}{Y_{oo}^b + Y_{oe}^b} = \frac{\sqrt{G G_A}}{Y_s + G} \quad (6)$$

$$N = \frac{2 G_A}{Y_{oo}^b - Y_{oe}^b} = \sqrt{\frac{G_A}{G}} \quad (7)$$

$$Y_{oo}^b = \frac{1}{\bar{Z}(1+a_{01})} \quad (8)$$

$$Y_{oe}^b = \frac{1}{\bar{Z}(1-a_{01})} \quad (9)$$

From eqs. (7), (8) & (9):

$$R = \frac{\bar{Z}^2}{R_A} \cdot \frac{(1 - a_{01}^2)^2}{a_{01}^2} \quad (10)$$

Equal width condition:

$$a_{01} = a_{10} = \sqrt{\frac{R_A}{R}} \quad \text{(special case)}$$

$$B_{0,1}^{c,s} = -\frac{1}{\gamma_1 \bar{Z}(1 - a_{01}^2)\tan\phi} \quad (11)$$

where

$$\gamma_1 = \frac{1}{1 - \frac{R_A}{\bar{Z}} \cdot \frac{a_{01}^2}{1 - a_{01}^2}} \quad (12)$$

$$X_s = \frac{X_A X_B}{X_A + X_B} \quad (1)$$

$$B_L = -\frac{1}{X_A + X_B} \quad (2)$$

$$T = \frac{X_B}{X_B + X_A} \quad (3)$$

$$R = \frac{R_A}{T^2}\left[1 + \left(\frac{X_s}{R_A}\right)^2\right] \quad (4)$$

$$B_o^c = -\frac{X_s}{R_A}\left[\frac{1}{R} + \frac{R_A T(1-T)}{X_s^2}\right] \quad (5)$$

$$X_A = \frac{X_s}{T} \quad (8)$$

$$X_B = \frac{X_s}{1-T} \quad (9)$$

SPECIAL CASE: $T = 1$ $(C_B = 0, X_s = X_A)$

$$R = R_A\left[1 + \left(\frac{X_A}{R_A}\right)^2\right] \quad (6)$$

$$B_o^c = -X_A\left[\frac{1}{R R_A}\right] \quad (7)$$

Fig. 3. Design relationships for (a) the parallel-coupled and (b) capacitive-tapped end inverters.

requires a change of resonator stub lengths; thus with this condition, one degree of design flexibility is lost. But with all linewidths equal, the product design becomes simpler.

With the use of the capacitive-tapped end section, gap tolerance problems are reduced. On the other hand, the capacitive transformation is more frequency dependent, thus narrowing the useful bandwidth to some extent. This frequency dependence sometimes causes excessive ripple at the lower band edge. (The ideal transformer representation of this end section is based on an earlier study by Page [9] and has been widely used everywhere.) The turns ratio $T$ is frequency independent, while $X_s$ is frequency dependent. Equation (4) of Fig. 3(b) indicates that the lower the value of $X_s$ [defined by (1)] the more constant $R$ becomes. (In this respect, $X_s$ is analogous to a leakage reactance.)

Using the special case of $T = 1$, the useful band is narrower than in the four capacitor case. But the resulting filter structure is a very simple one and quite useful for narrow-band applications. This design was already proposed by Crystal for a general combline structure [8].

It is helpful to distinguish between intermediate and end or external resonant nodes. End nodes are those with $j = 1$ and $n$, while intermediate nodes are with $j = 2 \cdots n - 1$ inclusive. All elements enclosed by the end nodes are called *intermediate* elements. Fig. 2 illustrates these ideas for type I and II filters.

Intermediate elements are discussed and defined in detail in the Appendix. While all intermediate elements are the same for all filter types, the end sections and nodes are different.

To interface with the intermediate nodes, both types of end nodes are characterized separately. Consider first the parallel-coupled end section of Fig. 3(a). Stub "$a$" is at node 0 while stub "$b$," characterized as $\bar{Z}$, is at resonant node 1. The sum of self and coupled susceptances from node 0 is given by (11) of the figure. Noting that the coupled susceptance from the internal resonator is given as $-a_{12}^2/\bar{Z}(1 - a_{12}^2)\tan\phi$, we obtain $y_{1T}$. The resonant node susceptance is then

$$B_1 = \frac{\tan\theta}{Z_1} - \left(\frac{1}{\gamma_1}\right)\frac{1}{\bar{Z}\tan\phi[1 - (a_{01}^2 + a_{12}^2)]}. \quad (1)$$

$b_1$ is obtained similar to (A12):

$$b_1 = \left(\frac{1}{\gamma_1}\right)\cdot\frac{F(\theta,\phi)}{2\bar{Z}\tan\phi[1 - (a_{01}^2 + a_{12}^2)]}$$

where

$$F(\theta,\phi) = \frac{2\theta}{\sin 2\theta} + \frac{2\phi}{\sin 2\phi}. \quad (2)$$

For the equal width condition, $a_{01} = a_{10} = (R_A/R^\circ)^{1/2}$. Substituting this into (10) of Fig. 3(a) and neglecting

$a_{12}^2$, $\bar{Z}^\circ = R^\circ R_A/(R^\circ - R_A)$ is obtained. Then $\gamma^\circ = 1/(1 - (R_A/R^\circ))$ from (12) of Fig. 3(a). From the results we conclude $\gamma^\circ \cdot (1 - a_{01}^2) = 1$. Thus

$$B_{0,1}{}^{c,s} = -1/(\bar{Z} \tan \phi)$$

which is the self susceptance. For this case, therefore, the coupled susceptances from nodes 0 and $n + 1$ are zero and only the coupled susceptances from the intermediate nodes are present. The resulting resonant node parameters are

$$B_1 = \frac{\tan \theta}{Z_1} - \frac{1}{\bar{Z}^\circ \tan \phi(1 - a_{12}^2)} \tag{3}$$

$$b_1 = \frac{1}{2\bar{Z}^\circ \tan \phi(1 - a^2{}_{12})} F(\theta, \phi). \tag{4}$$

For the capacitive-tapped section of Fig. 3(b), $B_0{}^c$ and $B_{n+1}{}^c$ are interpreted as the coupled susceptances from end nodes 0 and $n + 1$. Thus a resonant node is formed by adding $B_0{}^c$ to $B_{1,2}{}^{s,c} = 1/(\bar{Z} \tan \phi(1 - a_{12}^2))$ and resonating it with an open line for "$a$" type filters:

$$B_1 = \frac{\tan \theta}{Z_1} - \frac{1}{\bar{Z} \cdot \tan \phi \cdot (1 - a_{12}^2)} + B_0{}^c. \tag{5}$$

At resonance, (5) can be rearranged to give

$$\frac{\bar{Z}}{Z_1} = \frac{1}{\tan \theta \cdot \tan \phi \cdot (1 - a_{12}^2)} \cdot c \tag{6}$$

where $c = 1/(1 + k \cot \theta)$ and $k = B_0{}^c \cdot Z_1$.

The slope parameter is

$$b_1 = \frac{1}{2\bar{Z} \cdot \tan \phi \cdot (1 - a_{12}^2)} \cdot F(\theta, \phi, c) \tag{7}$$

where

$$F(\theta, \phi, c) = \frac{2\phi}{\sin 2\phi} + \frac{2\theta}{\sin 2\theta} \cdot c. \tag{8}$$

In deriving (7), the term $(\omega_0/2) \cdot dB_0{}^c/d\omega$ was dropped since its contribution to $b_1$ is considered negligible in most cases.

For the general case of unequal terminations $B_0{}^c \neq B_{n+1}{}^c$, therefore, $c$ takes on two values. This results in double values for $\bar{Z}$ which is also contradictory to the fundamental postulate 1 stated in the Appendix. To overcome this dilemma the average value of $c_1$ and $c_2$: $\bar{c}$ is used rather than either one of them. The same approach is taken to compute $\bar{\gamma}$ and $\bar{a}$ from (8) and (9) of Table II. This approach may not be feasible in some situations; fortunately, $\bar{Z}$ is a relatively weak function of termination differences since these constants have a limited effect on it. For equal terminations, of course, $\bar{c} = c_1 = c_n$, $\bar{\gamma} = \gamma_1 = \gamma_n$, etc.

Substitution of the lumped element components, slope parameters, and admittance inverters into these relationships and solving for the unknown parameters give the desired equations of Tables II and III.

In the derivation of coupling factors, (12) of Table II and (13) of Table III, the approximation

$$\frac{1 - a_{j,j+1}^2}{\{[1 - (a_{j-1,j}^2 + a_{j,j+1}^2)] \cdot [1 - (a_{j,j+1}^2 + a_{j+1,j+2}^2)]\}^{1/2}} \cong 1 + \tfrac{1}{2}(a_{j-1,j}^2 + a_{j+1,j+2}^2)$$

is used. Further comments on the tabulated equations are the following.

Some of the unknowns appear both as dependent and independent variables. These unknowns at the right sides of the equations are taken to be zero at the first computation of $\bar{Z}$, $a_{01}$, etc. Then the computation process is reiterated to obtain more precise values. In general, six iterations give precise solutions to the sixth decimal point.

Utilizing the equations in Table II, for type II filters, for example, these design steps are as follows.

1) Choose $\theta$, $\phi$, and $R$. Take $\gamma = 1$ and compute all parameters 1–15.

2) Use the results of step 1 to recompute parameters to be iterated for the required precision.

3) Solve for all tuning line impedances ($Z_j$) or capacitances ($C_j$) from (16) of Table II.

4) Solve for all even–odd mode impedances using (17) of Table II.

5) For dimensions of the coupled resonator stubs use the data of Bryant and Weiss [5]; for the tuning lines, refer to [6].

To compute gap spacing for the unequal width case, a method described by Crystal in [10] can be used. If the equal width condition is chosen then the choice of $\theta$ and $\phi$ defines the values of $R^\circ$ and $Z^\circ$. If unlike terminating impedances are used in the type I design, then both $T_1$ and $T_n$ should be computed.

At higher frequencies, capacitive tapping can be realized by transmission lines as shown in Fig. 4(a). $C_{A1}$ and $C_{An}$ are realized by a gap coupling at the first and last resonators. The gap discontinuity is effectively a capacitive Pi network; the values of such a network have been computed as a function of geometry for $w/h = 0.5$, 1.0, and 2.0 [11]. For higher capacitances the gap can be inter-

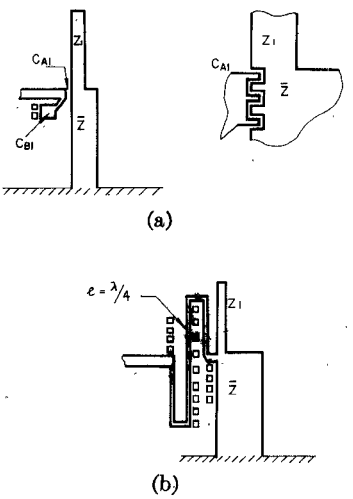


Fig. 4. Realization of end inverters at higher frequencies. (a) Capacitive tapping using open end shunt line for $C_B$ and gap discontinuity for $C_A$. Interdigitation shown at the right increases the effective capacitance of $C_A$. (b) Quarter-wave line end impedance transformer with fine tuning tabs along the line.

digitated; this increases the effective coupling length and the effective capacitance.

$C_{B1}$ and $C_{Bn}$ are realized by two open circuited low impedance lines paralleled in essence with the terminating impedances. Some adjustment can be provided here by trimming the length of these lines for the proper response.

Another form of end coupling is the use of the $\lambda/4$ line for uptransformation as on Fig. 4(b). Here, fine adjustment is realized by using tabs at both ends and alongside the line. For this case the line parameters are such that $Z_{01} = (R * R_A)^{1/2}$ and $Z_{0n} = (R * R_B)^{1/2}$. This transformation is quite effective for bandwidths over 20 percent.

## III. DESIGN EXAMPLES AND TEST RESULTS

Based on the equations of Tables II and III, two filters, one three pole and one four pole, were designed.

Of these two, the three-pole filter was built and tested. Mechanical data of the filter with photo and substrate metallization are shown in Fig. 5; performance data with computed and measured characteristics are given on Fig. 6. The terminating impedances are transformed up with two series capacitors making it a type I filter with the special case of $T = 1$. In this respect, the filter is a microstrip version of the type discussed in [8]. All three tuning lines are parallel, introducing some stray coupling and causing some increase in bandwidth. To obtain the specified bandwidth of between 12 and 16 percent, the original design started out with 9 percent, resulting in 13.5-percent bandwidth. The performance was good enough that no iterations were needed; the tuning lines had to be shortened by about 7 percent to obtain the correct center frequency. The computed response shows two notices at the upper stopband due to the transmission zeros introduced by the coupled resonators and uncoupled line stubs. Fine tuning is accomplished with high dielectric alumina segments. These segments are positioned on the resonator stubs for the best response during alignment. After completion of the alignment, they are bonded on the substrate surface with $Q_{max}$ or other low loss cement. With this method, tuning becomes a simple and quick process.

The filter substrate was tested in a launcher. Test results showed satisfactory performance. The 0.3-dB midband loss and 70-dB ultimate attenuation were encouraging, better than expected. The 0.3-dB midband loss corresponds to a circuit $Q$ of about 420.

The four-pole filter was not built but designed only to test the theory. The bandwidth came out exactly 9.0 percent as design called for. The VSWR is slightly in excess of the specified 1.98 near one band edge; this is due to narrow-band effects. The bandpass response is shown on Fig. 7 along with design data and tabulation of $\bar{Z}$ values as a function of number of iterations. It is seen that $\bar{Z}$ converges rapidly to its final value where it is precise to the seventh digit.

A computer flow chart is shown on Fig. 8 outlining the iterative computation process. $\bar{Z}$ is used as the pilot variable. One can get as close to the solution as wished by assigning a circle of convergence with radius $\delta$. Computation is completed when the magnitude increment of $\bar{Z}$ is such that it falls within the circle thus converging to a solution. A "safety exit" is provided from the loop in case the wrong data are fed in and convergence cannot be obtained. This is shown in statement block 8, where the iteration limit is set at 10.

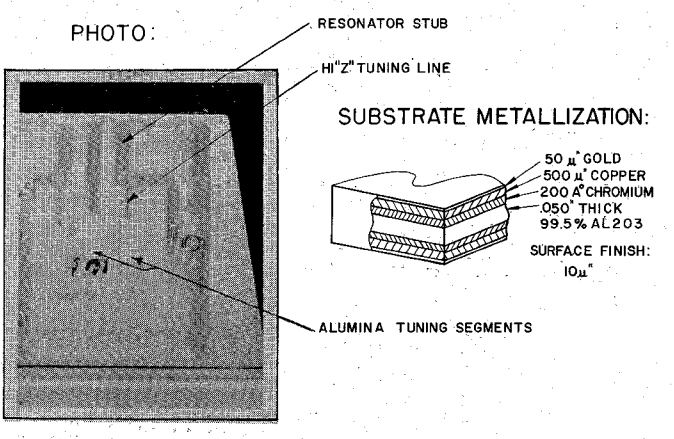


Fig. 5. Experimental three-pole filter mechanical data.

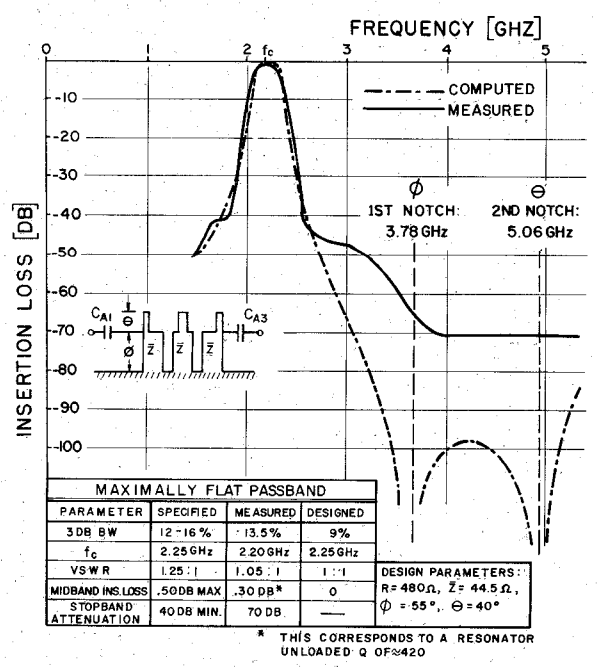


Fig. 6. Experimental three-pole filter performance data.

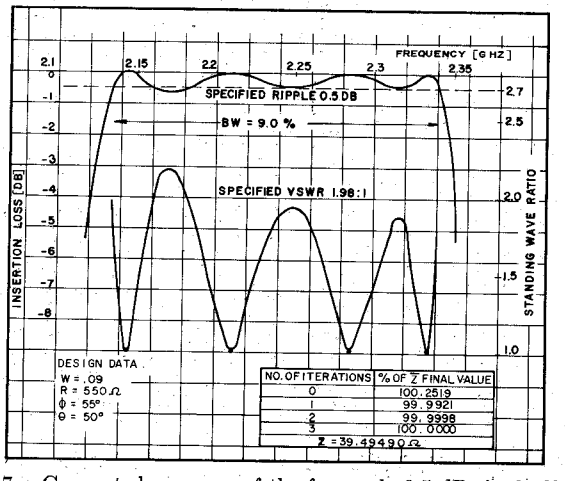


Fig. 7. Computed response of the four-pole 0.5-dB ripple filter.

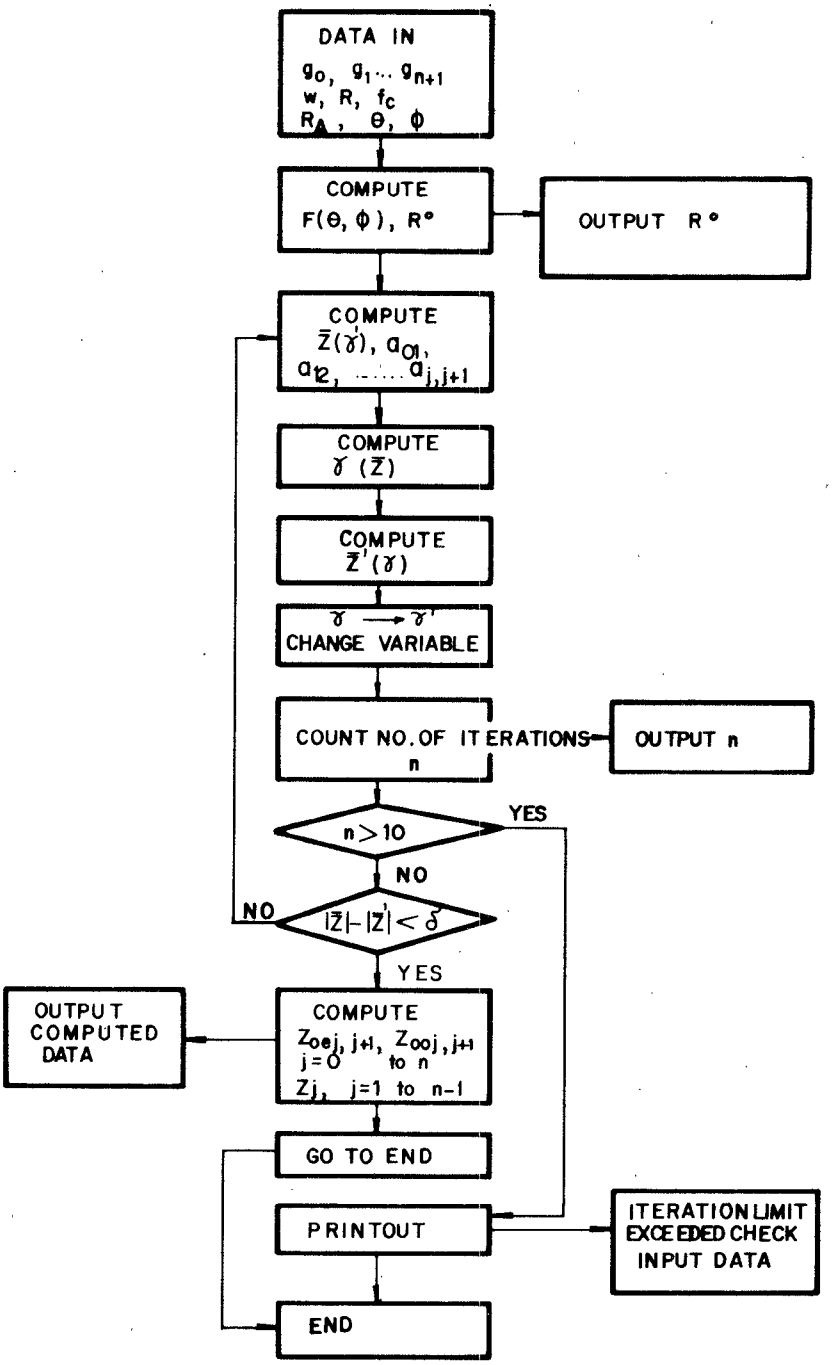


Fig. 8. Computer flow chart for type II filter design.

The first printout contains the type II special case parameter $R^\circ$. Then the number of iterations equal to $n$ is printed with all other design parameters.

The program is easily adaptable both to Basic and Fortran language.

## IV. SUMMARY

The semilumped element equivalent model of a combline-type filter for microstrip applications was developed with two configurations corresponding to the type I (capacitive end sections) and type II (parallel-coupled end sections) structures. It was seen that with this model simple formulas were developed in terms of even–odd mode impedances easily adaptable to microstrip design. The fundamental relationships were developed in the Appendix for the intermediate nodes. The end nodes were characterized at resonance for each special case associated with both type I and II filters. All equations are tabulated for convenience.

Test data of a three-pole filter show good results. The filter, besides being small in size, has good stopband attentuation of 70 dB which is attributed to the combline-type filter characteristics. The low midband loss of 0.30 dB could be the combined result of good substrate material and well chosen impedance levels.

The computed bandpass response of a four-pole 0.5-dB ripple filter is also shown with a computer flow chart to indicate some of the more significant statement blocks. The results show good agreement between theory and design.

## APPENDIX
## FUNDAMENTAL RELATIONSHIPS

Combline structures consist of parallel line pairs coupled to each other. Consider a pair of such lines represented by the $4 \times 4$ impedance matrix (Fig. 9):

$$\begin{bmatrix} V_1 \\ V_2 \\ 0 \\ 0 \end{bmatrix} = \begin{bmatrix} Z_{11} & \cdots & Z_{14} \\ \cdot & \cdots & \cdot \\ \cdot & \cdots & \cdot \\ Z_{41} & \cdots & Z_{44} \end{bmatrix} \times \begin{bmatrix} I_1 \\ I_2 \\ I_3 \\ I_4 \end{bmatrix}. \tag{A1}$$

Assume a symmetrical line pair. $I_3$ and $I_4$ are eliminated and the matrix is reduced to give the $2 \times 2$ form valid for two-port networks:

$$\begin{bmatrix} V_1 \\ V_2 \end{bmatrix} = \begin{bmatrix} z_{11} & z_{12} \\ z_{21} & z_{22} \end{bmatrix} \times \begin{bmatrix} I_1 \\ I_2 \end{bmatrix}$$

where

$$z_{11} = z_{22} = j\bar{Z} \tan \phi$$
$$z_{12} = z_{21} = ja\bar{Z} \tan \phi. \tag{A2}$$

The coefficients of (A1) represent even–odd mode impedance according to [1]. Equation (A2) was obtained by noting that

$$\frac{Z_{14}}{Z_{11}} = \frac{Z_{13}}{Z_{12}} = \frac{Z_{24}}{Z_{21}} = \frac{Z_{23}}{Z_{22}} = \sec \phi$$

and

$$1 - \sec^2 \phi = -\tan^2 \phi.$$

Let the following parameters be defined:

$$\bar{Z} = \frac{Z_{0e} + Z_{00}}{2} = \text{average mode impedance} \tag{A3}$$

$$a_{12} = \frac{Z_{0e} - Z_{00}}{Z_{0e} + Z_{00}} = \text{coupling factor.} \tag{A4}$$

Relating to the parameters defined by (A3) and (A4), the following fundamental postulates are stated.

1) The width of every resonator is kept the same. As a consequence, $\bar{Z}$ becomes unique single valued for one particular design. The constancy of $\bar{Z}$ is verified by the plot of Fig. 10 which is based on the information of [5]. For the curve, $W/H = 0.6$ is held as a constant parameter, resulting in the constancy of $\bar{Z}$ that appears as a horizontal line. This constancy is shown for the range $1.5 < S/H < 4.0$.

2) The spacing between resonators is varied making the coupling factor "$a$" different for the resonator pairs if design conditions dictate so. These postulates are summed up in the equation

$$Z_{0e12} + Z_{0012} = \frac{Z_{0e12} - Z_{0012}}{a_{12}} = 2\bar{Z}. \tag{A5}$$

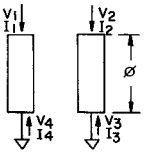


Fig. 9. Parallel-coupled symmetrical line pair.

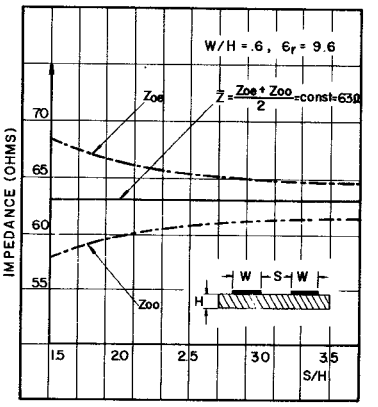


Fig. 10. Plot showing the constancy of $\bar{Z}$ versus $S/H$ for $W/H = 0.6$ for a pair of coupled microstrip lines (based on [5]).

For convenience, $z_{11}$ and $z_{12}$ are converted to $y$ parameters giving the susceptances

$$y_{11} = \frac{1}{\bar{Z} \tan \phi(1 - a_{12}^2)} = y_{22} \tag{A6}$$

$$y_{12} = \frac{a_{12}}{\bar{Z} \tan \phi(1 - a_{12}^2)} = y_{21}. \tag{A7}$$

Fig. 11 is the Pi-network representation of a two-port network characterized by $y$ parameters. The resulting network may be interpreted as a pair of resonators characterized by $y_{11}$ and coupled by a quarter-wave inverter with characteristic admittance $y_{12}$. (A detailed treatment on inverters is presented in [3, pp. 193–194].)

The ideas expressed in (A1)–(A7) are extended now to "$n$" pole filter structures. First the self admittance ($y_{11}^s$) is recognized and then the admittance components coupled from left ($y_{j-1}$) and right ($y_{j+1}$) are computed; the sum of these admittances form a resonant node.

The following assumptions are used. Assumption 1) is an extension of the fundamental postulates.

1) All resonator stubs for $j = 1 \cdots n$ have equal widths ($\bar{Z}$ = constant) resulting in symmetry of coupling coefficients, i.e., $a_{j,j+1} = a_{j+1,j}$. This may be interpreted in practical terms to mean that the coupling coefficient measured at either side of a coupled line pair has the same value.

2) Stray coupling between a resonator stub and the one beyond its nearest neighbor is neglected.

3) Coupling between the high impedance tuning lines is neglected.

Consider node $j$. If the resonators from left (node $j - 1$)

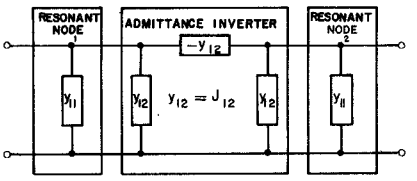


Fig. 11. Pi network equivalent of the symmetrical line pair of Fig. 9.

and right $(j+1)$ are far removed, $a_{j-1}$ and $a_{j+1}$ both become zero giving the self admittance $y_{11}^s = -j/\bar{Z}\tan\phi$ by (A6). $y_{11}$ of (A6) may be considered then as the sum of the self and one coupled node admittance. Applying this to node $j$ we may write

$$y_j = y_j^s + y_{j-1}^c, \qquad (y_j = y_{11}) \tag{A8}$$

from which the coupled admittance from node $j-1$ is

$$y_{j-1}^c = y_j - y_j^s = -j\frac{a_{j,j-1}^2}{\bar{Z}(1-a_{j,j-1}^2)\tan\phi}. \tag{A9}$$

Likewise, the coupled admittance from node $j+1$ is

$$y_{j+1}^c = -j\frac{a_{j,j+1}^2}{\bar{Z}(1-a_{j,j+1}^2)\tan\phi}. \tag{A10}$$

The total node admittance $y_j^T$ is the sum of $y_j^c$, $y_{j-1}^c$, and $y_{j+1}^c$. In general, for narrow-band design, all fourth order "$a$" products are disregarded. Then one obtains for $y_j^T$

$$y_j^T = -\frac{1}{\bar{Z}\tan\phi[1-(a_{j-1,j}^2+a_{j,j+1}^2)]}. \tag{A11}$$

A resonant node is formed by tuning out $y_j^T$ with a susceptance of equal magnitude and opposite sign. Physically, this is an open stub line of characteristic impedance $Z_j$ and electrical length $\theta$.

Thus the susceptance at node $j$ is

$$B_j = \frac{\tan\theta}{Z_j} - \frac{1}{\bar{Z}\tan\phi[1-(a_{j-1,j}^2+a_{j,j+1})]}. \tag{A12}$$

*Slope parameter* at node $j$ is defined as [7]

$$b_j = \frac{\omega_0}{2}\cdot\frac{dB_j}{d\omega}\bigg|_{\omega=\omega_0}. \tag{A13}$$

Using the definition of (A13) and noting that $B=0$ at $\omega=\omega_0$, one obtains $b_j$ from (A12):

$$b_j = \frac{1}{2\bar{Z}\tan\phi[1-(a_{j-1,j}^2+a_{j,j+1}^2)]}\cdot F(\theta,\phi) \tag{A14}$$

where

$$F(\theta,\phi) = \frac{2\phi}{\sin 2\phi} + \frac{2\theta}{\sin 2\theta}. \tag{A15}$$

*The admittance inverter* that couples the resonators at nodes $j$ and $j+1$ becomes from (A7)

$$J_{j,j+1} = \frac{a_{j,j+1}}{\bar{Z}\tan\phi(1-a_{j,j+1}^2)}. \tag{A16}$$

The resulting equivalent semilumped element representation of the filter structure is shown in Fig. 2.

Equations (A11)–(A16) are valid for nodes $j = 2\cdots n-1$. (The corresponding nodes are defined as *intermediate nodes.*) These equations will differ for the *end nodes* at $j=1$ and $n$. The reason being that the end impedance transforming sections introduce additional susceptance components to the end sections.

## ACKNOWLEDGMENT

The author wishes to thank R. Salazar for helpful technical suggestions, and H. F. Verse, A. H. Giddis, and Dr. E. W. Matthews for their support in carrying this idea to completion. He also wishes to thank his wife, Maria, for making all the illustrations and artwork. Finally, he wishes to thank E. Niemeyer for his efforts in testing and evaluating the experimental filter, and O. Bohrer and S. Lipp for their typing assistance.

## REFERENCES

[1] E. M. T. Jones and J. T. Bolljahn, "Coupled-strip-transmission-line filters and directional couplers," *IRE Trans. Microwave Theory Tech.*, vol. MTT-4, pp. 75–81, Apr. 1956.
[2] S. B. Cohn, "Parallel-coupled transmission-line-resonator filters," *IRE Trans. Microwave Theory Tech.*, vol. MTT-6, pp. 223–231, Apr. 1958.
[3] ——, "Direct-coupled-resonator filters," *Proc. IRE*, vol. 45, pp. 187–196, Feb. 1957.
[4] G. L. Matthaei, L. Young, and E. M. T. Jones, *Design of Microwave Filters, Impedance-Matching Networks and Coupling Structures.* New York: McGraw-Hill, 1964, ch. 4, 5, and 8.
[5] T. G. Bryant and J. A. Weiss, "Parameters of microstrip transmission lines and coupled pairs of microstrip lines," *IEEE Trans. Microwave Theory Tech. (1968 Symposium Issue)*, vol. MTT-16, pp. 1021–1027, Dec. 1968.
[6] W. Schilling, "The real world of micromin: Part III," *Microwaves*, pp. 57–59, 1969.
[7] G. L. Matthaei, "Combline band-pass filters of narrow or moderate bandwidth," *Microwave J.*, pp. 82–91, Aug. 1963.
[8] E. G. Crystal, "Capacity coupling shortens combline filters," *Microwaves*, pp. 44–50, Dec. 1967.
[9] D. F. Page, "A design basis for junction transistor oscillator circuits," *Proc. IRE*, vol. 46, pp. 1271–1280, June 1958.
[10] E. G. Crystal, "Coupled circular cylindrical rods between parallel ground planes," *IEEE Trans. Microwave Theory Tech.*, vol. MTT-12, pp. 428–439, July 1964.
[11] P. Benedek and P. Silvester, "Equivalent capacitances for microstrip gaps and steps," *IEEE Trans. Microwave Theory Tech.*, vol. MTT-20, pp. 729–733, Nov. 1972.